Opening the Higgs portal to lepton-flavoured dark matter

Harun Acaroğlu,[a] **Monika Blanke**[a,b] **and Mustafa Tabet**[c]

[a]*Institut für Theoretische Teilchenphysik, Karlsruhe Institute of Technology,*
Engesserstraße 7, D-76128 Karlsruhe, Germany

[b]*Institut für Astroteilchenphysik, Karlsruhe Institute of Technology,*
Hermann-von-Helmholtz-Platz 1, D-76344 Eggenstein-Leopoldshafen, Germany

[c]*Fakultät für Physik, Technische Universität Dortmund,*
Otto-Hahn-Straße, D-44221 Dortmund, Germany

E-mail: harun.acaroglu@kit.edu, monika.blanke@kit.edu,
mustafa.tabet@tu-dortmund.de

ABSTRACT: We study a simplified model of lepton-flavoured complex scalar dark matter coupling to right-handed leptons and the Higgs boson. The model is set up in the Dark Minimal Flavour Violation framework. In contrast to previous studies of similar models we consider the most general case and do not a priori constrain the hierarchy of dark matter masses and couplings in any way aside from the chosen parameter ranges. In the first part of the analysis we discuss the impact of Higgs portal interactions and the generalised mass hierarchy on the model's phenomenology. We find that they render new physics masses around the electroweak scale viable, thus qualifying this model to address the $(g-2)_\mu$ puzzle. After reviewing the current situation of the latter, we perform two combined analyses — one in which $(g-2)_\mu$ allows for significant new physics effects and one in which it does not. We find that while the latter scenario allows for a larger range of new physics scales, both scenarios are equally viable.

Contents

1   Introduction

The overwhelming evidence for the existence of Dark Matter (DM) in the Universe poses one of the major challenges to particle physics: its presence cannot be accounted for within the otherwise well-established Standard Model (SM), and thus its nature remains obscure. Numerous SM extensions have been proposed that address the issue, lacking however a direct experimental confirmation. For recent reviews, see e.g. [1, 2].

A popular approach to the DM problem is the WIMP hypothesis, i.e. the proposal that DM is a weakly interacting massive particle with mass around the electroweak (EW) scale. The DM is then produced via a thermal freeze-out, naturally leading to a relic abundance of the correct order of magnitude. Furthermore WIMP models are generally accessible to DM searches in direct and possibly indirect detection experiments as well as the Large Hadron Collider (LHC). The absence of a New Physics (NP) signal, on the other hand, puts simple WIMP models under severe pressure.

However, the introduction of a non-trivial flavour structure to the dark sector has been shown to significantly improve the situation [3–10]. The increased parametric freedom of flavoured DM models, in particular those that allow for a new source of flavour violation, allows to evade the tension between the required annihilation rate and the experimental non-observation of DM, thus making flavoured DM a viable WIMP candidate.

For an efficient study of flavoured DM beyond Minimal Flavour Violation [11–16], the concept of Dark Minimal Flavour Violation (DMFV) has been introduced [17], which minimally extends the model's flavour sector by allowing for a single new source of flavour violation. While earlier DMFV studies focussed mainly on quark-flavoured DM [17–21], the case of lepton-flavoured DM recently attracted increased attention [22–24] partially due to the long-standing anomaly in the anomalous magnetic moment of the muon, $(g-2)_\mu$ [25–28]. The first analysis of lepton-flavoured DM in DMFV considered the case of Dirac-fermionic DM and a scalar mediator [22]. NP contributions to $(g-2)_\mu$ were found negative, thereby increasing the potential tension between SM prediction and experiment. More recently, a DMFV model of complex scalar lepton-flavoured DM was proposed [23]. In this case, the NP contribution to $(g-2)_\mu$ has the right sign, however the combined constraint from the DM relic abundance and direct detection experiments pushed the new particles' masses in the TeV range, thus rendering them too heavy to have a relevant impact on $(g-2)_\mu$ or to be produced directly at the LHC. In ref. [24] the model was then extended to include DM couplings to both left- and right-handed leptons. In this way, the contribution to $(g-2)_\mu$ could be enhanced by a chirality-flip inside the NP loop, so that a NP resolution of the $(g-2)_\mu$ puzzle was possible. Yet it came at the cost of abandoning the DMFV minimality principle and of a significantly increased number of new parameters.

In the present paper we revisit the DMFV model of ref. [23] with the aim of identifying additional viable parameter space that allows to lower the NP spectrum to the EW scale. Such low masses make the model highly attractive for LHC searches, and they allow for a chirality-preserving NP resolution of the $(g-2)_\mu$ puzzle if eventually required. On the one hand, the Higgs portal interaction that is naturally present in singlet scalar DM models [29, 30] has been neglected in ref. [23]. On the other hand, the hierarchy among the dark flavours has been fixed such that the lightest flavour, i.e. the DM candidate, has the strongest coupling to the SM fermions. Here we relax both assumptions and explore the impact of non-vanishing Higgs portal interactions and of a reversed mass hierarchy in the dark sector on the model's phenomenology.

2 Theory

In this section we present the details of the model introduced originally in ref. [23] and studied in the subsequent analysis. Special emphasis is put on the Higgs portal interaction and on the DM mass spectrum, while we refer the reader to ref. [23] for further details on the flavour structure of the model.

2.1 Model setup and details

We introduce DM as a complex scalar field $\phi = (\phi_1, \phi_2, \phi_3)^T$ which transforms as singlet under the SM gauge group and as a triplet under the new approximate global flavour symmetry $U(3)_\phi$. This triplet is coupled to the right-handed leptons ℓ_R of the SM through a new Dirac fermion ψ, the so-called mediator. The latter carries the same gauge quantum numbers as ℓ_R, i.e. it transforms as a singlet under the $SU(2)_L$ and $SU(3)_C$ gauge groups of the SM and has a hypercharge of $Y = -1$. In order to stabilise DM, the new fields ϕ and ψ

are charged under a discrete $\mathbb{Z}_2$ symmetry. The Lagrangian of this model reads[1]

$$\mathcal{L} = \mathcal{L}_{\text{SM}} + (\partial_\mu \phi)^\dagger (\partial^\mu \phi) - \hat{M}_\phi^2 \, \phi^\dagger \phi + \bar{\psi}(i\slashed{D} - m_\psi)\psi - (\lambda_{ij} \bar{\ell}_{Ri} \psi \, \phi_j + \text{h.c.}) \\ - \Lambda_{H,ij} \, \phi_i^\dagger \phi_j \, H^\dagger H + \Lambda_{\phi,ijkl} \phi_i^\dagger \phi_j \phi_k^\dagger \phi_l \,. \tag{2.1}$$

The coupling matrix λ parameterises the lepton portal interaction. Following the DMFV assumption [17], λ constitutes the only new source of flavour and CP violation beyond the SM Yukawa couplings.

Additionally, ϕ also couples to the SM Higgs boson through the quartic coupling matrix Λ_H, the Higgs portal. Its most general form consistent with the DMFV assumption can be obtained adopting the spurion ansatz from MFV [12]. We thus parameterise the Higgs portal coupling matrix Λ_H in terms of the lepton portal coupling λ by writing

$$\Lambda_H = \lambda_H \left\{ \mathbb{1} + \eta_H \left(\lambda^\dagger \lambda \right) + \mathcal{O}(\lambda^4) \right\} . \tag{2.2}$$

Here λ_H is a flavour-universal coupling parameter, and the $\mathcal{O}(\lambda^2)$ correction is induced by effects from the UV completion.[2] Our ignorance about the latter is accounted for by the new parameter η_H.

Following ref. [23] we decompose the coupling matrix λ as

$$\lambda = UD \tag{2.3}$$

where D is a diagonal matrix with positive real entries D_i, and U is a unitary matrix parameterised by three mixing angles θ_{ij} and three complex phases δ_{ij}. The explicit form of the parameterisation has been adopted from ref. [31] and can be found in ref. [23]. Note that we made use of the $\text{U}(3)_\phi$ flavour symmetry to reduce the number of free parameters in λ to nine. Reinserting this expression for the lepton portal coupling matrix λ into the expression from equation (2.2) for Λ_H we find

$$\Lambda_H = \lambda_H \left\{ \mathbb{1} + \eta_H \, D^2 + \mathcal{O}(D^4) \right\} , \tag{2.4}$$

i.e. the coupling matrix Λ_H is diagonal when maintaining the DMFV hypothesis.

In summary, the two coupling matrices λ and Λ_H contain a total number of eleven physical parameters for which we adopt the following ranges to avoid a double-counting of the parameter space and ensure perturbativity:

$$\theta_{ij} \in \left[0, \frac{\pi}{4}\right], \quad \delta_{ij} \in [0, 2\pi], \quad D_i \in [0, 3], \quad \lambda_H \in [-3, 3], \quad \eta_H \in [-0.1, 0.1]. \tag{2.5}$$

Within these ranges the DMFV corrections to the Higgs portal coupling can grow as large as ± 0.9 indicating that higher-order terms in the DMFV expansion may become important. The results of our analysis show, however, that the size of the Higgs portal interaction is severely constrained phenomenologically, and we therefore consider it sufficient to include only the leading DMFV correction. In passing we note that, following a similar procedure, also the DM quartic coupling Λ_ϕ can be written in terms of a DMFV spurion expansion. Since, however, this coupling has no practical implications for our analysis, we do not consider it further.

---

[1] We caution the reader to not confuse the dimensionless coupling matrices Λ_H and Λ_ϕ with energy scales.

[2] Note that loop corrections within the simplified model arise only at higher order in the DMFV spurion expansion.

2.2 Mass spectrum

In analogy to the Higgs portal coupling matrix Λ_H, the DM mass matrix $\hat{M}_\phi^2$ also cannot be an arbitrary 3×3 matrix as this would violate the DMFV hypothesis. Again, following ref. [23] we adopt the DMFV spurion expansion and write

$$\hat{M}_\phi^2 = m_\phi^2 \left\{ \mathbb{1} + \eta \left(\lambda^\dagger \lambda \right) + \mathcal{O}\left(\lambda^4 \right) \right\} = m_\phi^2 \left\{ \mathbb{1} + \eta\, D^2 + \mathcal{O}\left(D^4 \right) \right\} . \tag{2.6}$$

The flavour non-universal corrections are due to one-loop renormalisation contributions already present in the simplified model and/or induced by the UV completion of the theory. Their unknown size is parameterised by the expansion parameter η in equation (2.6) which we restrict to the range $|\eta| < 0.1$, while m_ϕ^2 is the flavour-universal leading order mass parameter.[3]

Additionally, the interactions in the Higgs portal induce contributions to the DM mass matrix $\hat{M}_\phi^2$ due to electroweak symmetry breaking (EWSB). These corrections are proportional to Λ_H, and yield the physical mass matrix

$$M_\phi^2 = \hat{M}_\phi^2 + v^2 \Lambda_H , \tag{2.7}$$

where $v = 174\,\mathrm{GeV}$ is the Higgs vacuum expectation value (vev).

Inserting the expressions for Λ_H from equation (2.4) and $\hat{M}_\phi^2$ from equation (2.6) into equation (2.7) we then find

$$M_\phi^2 = \left(m_\phi{}^2 + \lambda_H v^2 \right) \left\{ \mathbb{1} + \left(\eta + \frac{v^2\, \lambda_H\, (\eta_H - \eta)}{m_\phi{}^2 + \lambda_H v^2} \right) D^2 + \mathcal{O}(D^4) \right\} , \tag{2.8}$$

for the resulting physical mass matrix M_ϕ^2. We see that M_ϕ^2 exhibits the DMFV expansion pattern, as expected.

We additionally adopt the convention of ref. [23] to order the fields ϕ_i in such a way that the mass matrix M_ϕ^2 satisfies the hierarchy condition

$$M_\phi^2 = \mathrm{diag}\left(m_{\phi_1}^2, m_{\phi_2}^2, m_{\phi_3}^2 \right) , \tag{2.9}$$

with $m_{\phi_1} > m_{\phi_2} > m_{\phi_3}$. Complemented by the condition that ϕ_3 be lighter than the mediator ψ, this renders ϕ_3 the lightest of all new states and we assume it to account for the observed amount of DM in the Universe.

Finally, as mentioned above we impose a $\mathbb{Z}_2$ symmetry under which only the new fields ϕ_i and ψ are charged. This ensures that neither of these fields can decay into SM particles only, and thus guarantees the stability of the DM candidate ϕ_3.

3 Phenomenology

The inclusion of the Higgs portal interactions of the DM triplet leads to significant changes in this model's phenomenology compared to the results of the study in ref. [23]. In this

---

[3]Note that in contrast to Λ_H the higher-order corrections to $\hat{M}_\phi^2$ may become relevant, since phenomenologically the parameter m_ϕ^2 is not constrained to be small. However, for consistency reasons we also truncate this expansion after the leading correction.

(a) DM-DM annihilation mediated by a Higgs in the s-channel

(b) DM-DM annihilation mediated by the four scalar vertex interaction

(c) DM-nucleon scattering mediated by a Higgs in the t-channel
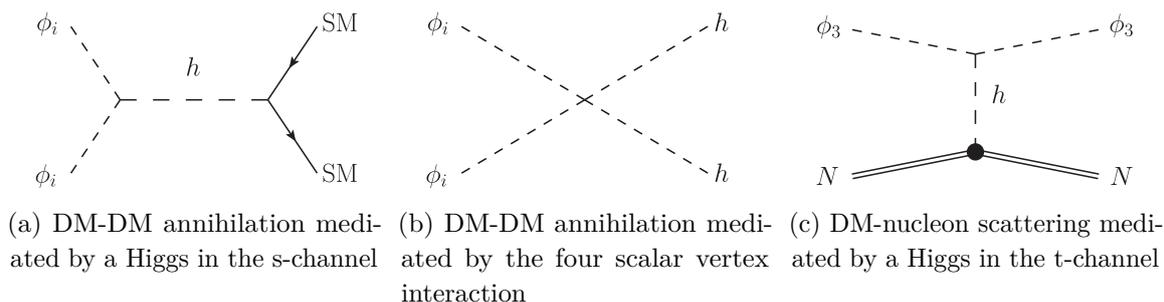
Figure 1. New processes due to the Higgs portal interactions. In the first panel from the left the final state consists of a pair of any SM particle the Higgs boson couples to. The panel in the middle shows the annihilation diagrams involving four scalar interactions proportional to the Higgs portal coupling Λ_H.

section we first provide an overview of how the phenomenology is altered by these additional interactions. We then we demonstrate how these changes render NP masses of the order of the EW scale viable and explore if this extended parameter space allows us to address the $(g-2)_\mu$ puzzle in this model.

3.1 Phenomenology of Higgs portal

Besides generating the additional mass corrections discussed in section 2.2, the Higgs portal interactions are mainly relevant for two aspects of the model's overall phenomenology as discussed in ref. [23]: DM detection experiments and the freeze-out of DM in the early Universe. Conversely, these interactions do not induce lepton-flavour violating (LFV) decays as the DMFV expansion from equation (2.2) yields a diagonal Higgs portal coupling matrix Λ_H. Regarding the model's LHC phenomenology, it was shown in ref. [23] that the relevant process here is the Drell-Yan production of mediator pairs $\bar{\psi}\psi$ that subsequently decay into DM and leptons through lepton portal interactions. Hence, the inclusion of Higgs portal interactions does not alter the model's phenomenology in this regard either. We will however see that the impact of the Higgs portal contributions to DM detection and production shown in figure 1 render small NP scales viable, such that constraints from additional observables become relevant and the new particles may be in reach of the LHC.

The quartic coupling Λ_H of the flavour triplet ϕ to the SM Higgs doublet gives rise to additional DM annihilation processes shown in figure 1(a) and figure 1(b), which are particularly relevant for its thermal freeze-out. These processes can yield significant contributions to the thermally averaged total annihilation rate $\langle \sigma v \rangle$ of DM in addition to the standard annihilation of two incoming particles $\phi_i^\dagger \phi_j$ into a pair of leptons $\bar{\ell}_k \ell_l$ through the exchange of the new mediator ψ in the t-channel. Also, in contrast to the p-wave suppressed latter processes [23], the annihilations shown in figure 1(a) and 1(b) proceed in the s-wave and can become resonantly enhanced at several thresholds in the regime of the electroweak scale. These enhancements either happen around the threshold $2m_{\phi_i} \approx m_h$, where the Higgs in the s-channel is produced resonantly, or where the mass of DM is equal to the Higgs, W, Z boson or the top quark mass [29]. Overall, the existence of

these additional processes and resonances allows for a substantially increased production of DM in the early Universe, ultimately rendering smaller NP couplings compatible with the constraints coming from the observed DM relic density than in the case studied in ref. [23].

Some additional Higgs portal annihilation channels however are also subject to constraints from indirect detection experiments. Here, the model parameters can be restricted on the basis of the cosmic-ray antiproton flux measured by the AMS-02 experiment, which in turn translates into limits on the annihilation rate of two dark particles ϕ_3 into a pair of W bosons, Z bosons or top quarks [32, 33]. The same process with positrons or tau leptons in the final state is in principle also subject to indirect detection constraints stemming from measurements of either the positron flux or the γ-ray continuum spectrum [23, 34]. However, due to the smallness of the lepton Yukawa couplings y_ℓ and the absence of resonances in the relevant mass regimes, these processes can be safely neglected.

Further constraints on the Higgs portal coupling Λ_H and the DM mass come from spin-independent DM-nucleon scatterings through the t-channel process shown in figure 1(c). In contrast to the scatterings governed by the lepton portal coupling λ which arise at the one-loop level, these scatterings proceed at tree-level and can hence become sizeable. Due to this new process, the spin-independent averaged DM-nucleon scattering cross section

$$\sigma_{\rm SI}^N = \frac{\mu^2 \, |Z f_p + (A - Z) f_n|^2}{\pi A^2} \,, \tag{3.1}$$

receives additional contributions [29]

$$f_{n/p}^h = \frac{\Lambda_{H,33} \, y_N}{2} \frac{m_N}{m_h^2 m_{\phi_3}} \,, \tag{3.2}$$

where $y_N \simeq 0.3$ is the Higgs-nucleon coupling, m_N is the nucleon mass and the reduced mass is given by $\mu = m_{\phi_3} m_N / (m_{\phi_3} + m_N)$. The lepton portal contribution to DM-nucleon scattering can be found in ref. [23].

Compared to the scenario studied in ref. [23], the interplay between these new processes extends the viable parameter space of the model to also include small mediator masses $m_\psi \approx v$. These masses were found to be excluded in ref. [23] since in that analysis not only was the Higgs portal interaction Λ_H neglected, but also only the case was considered where the lightest dark flavour ϕ_3 couples the most strongly to the SM. To ensure this hierarchy in the masses and couplings of the different dark flavours, the parameter η from equation (2.6) was chosen to be negative. Additionally only two discrete freeze-out scenarios were explored, in which either all dark flavours contribute equally to the freeze-out or only the lightest one does. Hence, the hierarchy of masses and couplings[4] was either forced to be quasi-degenerate or one coupling D_i was significantly larger than the other two, such that one mass m_{ϕ_i} was significantly smaller than the others. As a result of these assumptions, it was only possible to satisfy the constraints from the observed DM relic density and direct detection experiments simultaneously at large NP scales m_ψ. The reason is that the p-wave

---

[4]Remember that for negligible Higgs portal interactions the DM masses are connected to the lepton portal couplings through $m_{\phi_i}^2 = m_\phi^2 \left(1 + \eta D_i^2\right)$, see section 2.2.

suppression of the annihilation rate demands large couplings, which in both freeze-out scenarios are only compatible with constraints from direct detection at large NP scales.

In this work, however, we find that the existence of the additional annihilation channels shown in figure 1(a) and 1(b) and governed by the Higgs portal coupling changes this picture in favour of small NP scales. We show this result in figure 2, where we present the allowed parameter space in the m_{ϕ_3}–m_ψ mass plane for three distinct scenarios at 95% CL. To obtain these results we have employed the statistical procedure that we describe at the beginning of section 3.3. In order to allow for a direct comparison with figure 7.1 of ref. [23] we check constraints from LFV decays [35–37], the observed DM relic density [38], direct detection [39] and indirect detection experiments [34, 40, 41]. Note, however, that in contrast to the analysis in ref. [23] we do not limit the mass hierarchy between the three dark states in any sense and consider the most generic case.

The orange region in figure 2 shows the case where we neglect interactions in the Higgs portal and demand the lightest dark state to have the strongest coupling to the SM ($\eta < 0$), i.e. we reproduce[5] the case studied in ref. [23]. As explained above, we find that the interplay between constraints from the observed DM relic density and direct detection experiments forces the NP scale m_ψ to be comparably large. The only exception from this is the close-to-degenerate region with $m_\psi \approx m_{\phi_3}$, which also allows for NP masses as small as the electroweak scale. This is due to the fact that in this region the otherwise Boltzmann-suppressed processes of mediator-DM annihilation into a lepton and a Z or γ as well as the even further Boltzmann-suppressed mediator-mediator annihilation into a pair of leptons become relevant due to the small mass splitting. Hence, in this regime the correct relic abundance can be obtained with comparably small couplings such that constraints from direct detection can be fulfilled for small masses m_ψ.

The hatched region on the other hand shows the allowed parameter space for the case $\eta > 0$ and $\lambda_H = 0$. Changing the sign of η generally induces hierarchies where the lightest dark state has the smallest coupling such that constraints from direct detection experiments can be evaded. The correct relic density is then obtained through annihilations of the heavier states ϕ_1 and ϕ_2 alone. As one can see, this scenario thus allows for a wider range of NP masses, reaching from the highest scale we consider in our analysis down to the electroweak scale. The lower bound on the DM mass m_{ϕ_3} for a given value of m_ψ is due to the annihilation rate of $\phi_i^\dagger \phi_i \to \ell_k \bar{\ell}_k$ being proportional to $m_{\phi_i}^2 D_i^4 / m_\psi^4$. As we have limited the couplings to $D_i \in [0,3]$, for a given mediator mass m_ψ the DM mass m_{ϕ_i} may not become arbitrarily small, as this would result in a too small annihilation rate or too large relic density, respectively.

Finally, we also consider the most general case where we allow for abitrary values and signs of η while also opening the Higgs portal. The allowed masses for this scenario are shown by the blue region in figure 2. We find that due to the inclusion of Higgs portal interactions the viable parameter space is significantly extended. While new annihilation channels proportional to the Higgs portal coupling λ_H enhance the total DM annihilation

---

[5]Note however, that we use updated constraints on the spin-independent DM-nucleon scattering rate in our analysis.
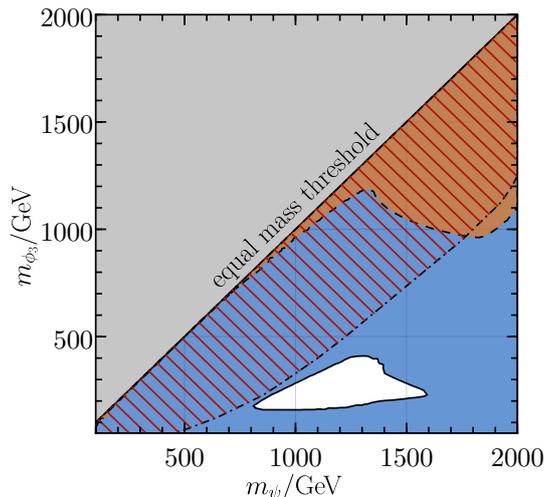
Figure 2. Allowed masses m_ψ and m_{ϕ_3} at 95% CL when satisfying constraints from LFV decays, the observed relic density, direct and indirect detection. The orange region shows the case with $\lambda_H = 0$ and $\eta < 0$, the hatched region the case with $\lambda_H = 0$ and $\eta > 0$, and the blue region the most general case with $\lambda_H \neq 0$ and an arbitrary η.

rate in the early Universe, the new contribution to DM-nucleon scattering induced by the Higgs portal can interfere destructively with the lepton portal contribution. Hence, in this scenario the interplay between relic density and direct detection constraints is much more dynamic, ultimately leading to the extended allowed parameter space. We find that except for a small region between $m_\psi = 800\,\text{GeV}$ and $m_\psi = 1600\,\text{GeV}$, the complete m_ψ–m_ϕ plane is rendered viable.

We conclude that in both new scenarios, i.e. a positive η with $\lambda_H = 0$ as well as arbitrary values for η with $\lambda_H \neq 0$, the viable parameter space of the model is significantly extended and allows for small mediator and DM masses. On the one hand, this result renders additional phenomenological constraints relevant, in particular from EW precision data and LHC searches. On the other hand, it implies sizeable NP effects in observables which ref. [23] had previously concluded to be insensitive to the model, due to the large mass scale found in that study. This applies in particular to collider searches and the muon anomalous magnetic moment $(g-2)_\mu$.

3.2 Muon anomalous magnetic moment

Ref. [23] found it impossible to address the potential anomaly between the measurement and theory prediction of the muon's anomalous magnetic moment in the scenario with $\eta < 0$ and $\lambda_H = 0$. This is due to the afore-mentioned interplay between constraints from the observed relic density of DM and direct detection experiments, which forces the NP scale m_ψ to be of order $\mathcal{O}(\text{TeV})$ in this scenario. The operator that gives rise to the muon's magnetic moment involves a chirality flip, and as the flavour triplet ϕ only couples to right-handed leptons in our model, sizeable NP effects in $(g-2)_\mu$ require NP masses at the electroweak scale, $m_\psi \sim \mathcal{O}(100\,\text{GeV})$. While in principle such small masses are also

viable in the case studied in ref. [23] within the near-degenerate region $m_\psi \approx m_{\phi_3}$, stringent constraints from searches for soft leptons exclude this part of the parameter space, as will be discussed in detail in section 3.3.

However, in section 3.1 we have seen that allowing for interactions in the Higgs portal or inverting the hierarchy between the couplings and masses of the flavour triplet ϕ renders small NP masses around the electroweak scale viable. This raises the question if sizeable NP contributions to $(g-2)_\mu$ can be generated in either of these scenarios, while satisfying all relevant experimental constraints. It should however be noted that while the experimental measurement of $(g-2)_\mu$ is uncontroversial [25–27], the corresponding SM theory prediction is subject to ongoing discussions and research. In ref. [28], the Muon $(g-2)$ Theory Initiative has presented a state-of-the-art prediction for $a_\mu = (g-2)_\mu/2$ where dispersive techniques are used to extract the leading-order hadronic vacuum polarisation (HVP) contribution from $\bar{e}e \to$ hadrons data.[6] Compared to the a_μ measurement, this data-driven prediction yields a difference between theory and experiment of

$$\Delta a_\mu^{\mathrm{exp,dat}} = a_\mu^{\mathrm{exp}} - a_\mu^{\mathrm{SM,dat}} = (2.49 \pm 0.48) \times 10^{-9} \,, \tag{3.3}$$

which corresponds to a discrepancy of 5.1σ.

In ref. [62], the BMW Lattice QCD collaboration has in turn presented a calculation of the HVP contribution to a_μ using a first-principle lattice QCD approach. Based on their results, the difference between the prediction and measurement of a_μ is reduced to

$$\Delta a_\mu^{\mathrm{exp,lat}} = a_\mu^{\mathrm{exp}} - a_\mu^{\mathrm{SM,lat}} = (1.05 \pm 0.62) \times 10^{-9} \,, \tag{3.4}$$

corresponding to a deviation of 1.6σ, which substantially eases the tension between theory and experiment. Recent results from other lattice groups are in agreement with the BMW result [63–66]. However, restricting the use of lattice data to the region least prone to systematic uncertainties and using data-driven techniques otherwise yields a result for the HVP contribution which only reduces the deviation between theory and experiment to 3.8σ [63, 67, 68]. Further, the discrepancy between the two approaches to determine the HVP contribution renders the lattice results incompatible with $\sigma\,(\bar{e}e \to$ hadrons$)$ data hinting at some unresolved issue in either of the approaches. The problem is exacerbated by the fact that the latest CMD-3 measurement of $\sigma\,(\bar{e}e \to \pi^+\pi^-)$ data is incompatible with previous determinations [69–73]. To provide an overview of this situation we summarise the numerical values of different SM predictions in appendix A.

In light of this situation, we consider it plausible that the resolution of this puzzle might require NP in a_μ. Hence, in our numerical analysis in section 3.3, we use the SM prediction of a_μ based on the HVP contribution obtained through dispersive techniques, i.e. we consider the scenario in which $\Delta a_\mu^{\mathrm{exp}}$ exhibits an anomaly. However, to keep track of any possible outcome of future settlements regarding the $(g-2)_\mu$ anomaly, in section 3.3 we also perform a combined analysis based on the BMW calculation and the resulting difference between theory and experiment as given in equation (3.4), i.e. we also consider the scenario in which $\Delta a_\mu^{\mathrm{exp}}$ is SM-like.

---

[6]See refs. [42–61] for relevant original work.

(a) NP contribution to a_μ (b) Z–ℓ vertex corrections
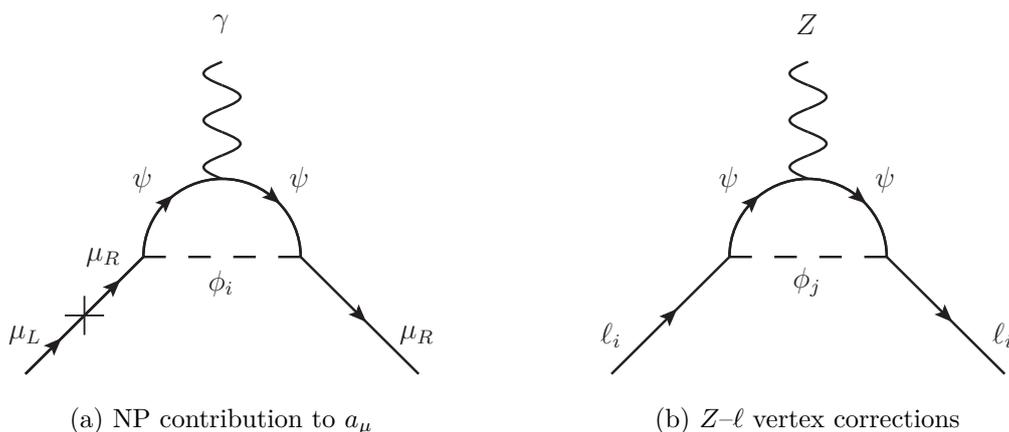
Figure 3. NP corrections to lepton-gauge-boson couplings. The left panel shows the NP contributions Δa_μ to the muon anomalous magnetic moment. The right panel shows vertex corrections to the Z–ℓ couplings.

In our model, the NP contribution Δa_μ to the anomalous magnetic moment of the muon is generated through the process shown in figure 3(a), i.e. the muon chirality needs to be flipped through a mass insertion on one of the external muon lines. It is given by

$$\Delta a_\mu = \frac{m_\mu^2}{16\pi^2} \sum_i \frac{|\lambda_{\mu i}|^2}{12 m_{\phi_i}^2} F(x_i) \,, \tag{3.5}$$

with $x_i = m_\psi^2 / m_{\phi_i}^2$ and the loop function F reads

$$F(x) = \frac{2}{(1-x)^4} \left[2 + 3x - 6x^2 + x^3 + 6x \ln x \right] . \tag{3.6}$$

We stress that in addition to the constraints considered in ref. [23], i.e. constraints from collider searches, LFV decays, the observed DM relic density and direct and indirect DM detection experiments, at scales $m_\psi \sim \mathcal{O}(100\,\mathrm{GeV})$ it is necessary to also include limits coming from other experiments. Besides similar NP contributions Δa_e to the anomalous magnetic moment of the electron, the most important constraints stem from the Z–ℓ vertex corrections shown in figure 3(b). Given that we allow for new interactions in the Higgs portal, we also need to consider new constraints related to the Higgs sector. For sufficiently small DM masses $m_{\phi_3} < m_h/2$ we hence include limits from invisible Higgs decays shown in figure 4(a). While loop corrections to the lepton Yukawa couplings shown in figure 4(b) are in principle also constrained, we will find in section 3.3 that in light of direct detection and relic density constraints the Higgs portal coupling needs to be suppressed. Hence, the h–ℓ vertex corrections, which are additionally suppressed by a loop factor and their proportionality to the lepton mass, can safely be neglected.

3.3 Combined analysis

In this section, we perform a global analysis and determine our model's allowed parameter space by considering all relevant constraints simultaneously. While we particularly discuss

(a) invisible Higgs decay   (b) h–ℓ vertex corrections
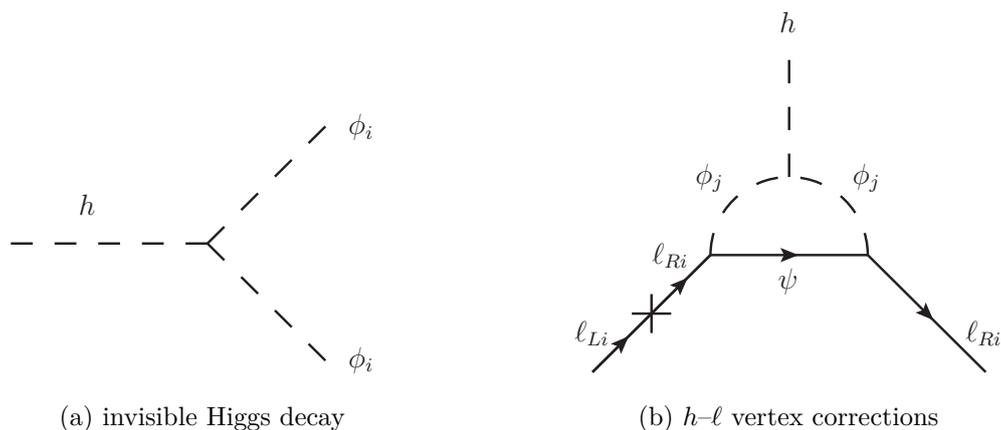
Figure 4. Additional processes due to Higgs portal interactions.

the feasibility of generating large enough NP effects in a_μ to reproduce $\Delta a_\mu^{\mathrm{exp,dat}}$, following our discussion from the last section, we also discuss the scenario where $(g-2)_\mu$ is in agreement with its SM prediction, i.e. we impose $\Delta a_\mu^{\mathrm{exp,lat}}$ as a constraint in the fit.

Technical details. In order to quantify the agreement between the data and our model, we employ χ^2-statistics. Thus, in order to determine the best-fit point, we minimise the function

$$\chi^2 = \left(\vec{\mathcal{O}}_{\mathrm{th}}(\xi_i) - \vec{\mathcal{O}}_{\mathrm{exp}}\right)^T C^{-1} \left(\vec{\mathcal{O}}_{\mathrm{th}}(\xi_i) - \vec{\mathcal{O}}_{\mathrm{exp}}\right) , \qquad (3.7)$$

where the vector $\vec{\mathcal{O}}_{\mathrm{th}}(\xi_i)$ contains the theory predictions as a function of the model parameters ξ_i, and the corresponding experimental measurements with the covariance matrix C are denoted by the vector $\vec{\mathcal{O}}_{\mathrm{exp}}$. For the case that this model is realised in nature, one can further determine confidence intervals for the model parameters around the best-fit point at a given confidence level. We consider constraints from collider searches [74–76], the observed DM relic density [38], direct detection [39], indirect detection [33, 34, 40, 41], the anomalous magnetic moment of the electron [77–79], Z–ℓ vertex corrections [80], and invisible Higgs decays [81]. We do not include constraints from LFV decays into our fit, since we limit our analysis to the flavour-conserving case with $\theta_{ij} = 0$. Note that including flavour-violating interactions would only increase the available parameter space and not change our conclusions qualitatively.

Some experiments only provide upper limits. In that case, we convert the upper limits into central values and uncertainties assuming Gaussian distributions centered around zero in order to include them into the χ^2-function from equation (3.7). Since the experimental uncertainty for the DM relic density is very small [38], we further include an uncertainty of 10 % on our theory prediction. The latter has been evaluated in a private fork of `micrOMEGAs` [82] in order to speed up the evaluation. The relic densities obtained in our analysis have been validated against the publicly available version.

Since the collider constraints are crucial in the mass region we are interested in, we perform a full recast. As discussed above and in ref. [23] the most important collider

signatures are the ones with two final state leptons and missing transverse energy. However, since no dedicated searches for this final state in our model are available, one can put limits on the parameter space by recasting supersymmetry searches with final state leptons and neutralinos. Depending on the mass splitting between the mediator and the invisible particles in the final state, different searches become important.

For large mass splittings, the strongest constraint comes from ref. [76] where a search for the signature $pp \to \bar{\ell}\ell\chi_1^0\tilde{\chi}_1^0$ with $\ell = e, \mu$, has been performed on the full Run 2 dataset with an integrated luminosity of $137\,\mathrm{fb}^{-1}$ at a center of mass energy of $\sqrt{s} = 13\,\mathrm{TeV}$ by the CMS experiment. A similar search [75] has been performed by the ATLAS experiment on a dataset of $139\,\mathrm{fb}^{-1}$ collected at $\sqrt{s} = 13\,\mathrm{TeV}$. While the CMS search is important for larger mass splittings, this search becomes important for mass splittings near the W boson mass. Finally, in the soft mass region, i.e. small mass splittings, the CMS search for two soft oppositely charged leptons and missing transverse momentum [74] at $\sqrt{s} = 13\,\mathrm{TeV}$ on a dataset of $35.9\,\mathrm{fb}^{-1}$ becomes relevant. The search has been performed for the production and decay of an electroweakino pair and of a chargino-mediated stop pair where in our case only the former one is of interest.

To recast these searches, we generate $pp \to \phi_i\phi_j^\dagger\bar{\ell}\ell$ in the four flavour scheme at leading order in `MadGraph5_aMC@NLO` [83]. For this, we have implemented the Lagrangian in equation (2.1) in `FeynRules` [84] and generated a `UFO` file. The events are fed into a standalone version of `PYTHIA 8.3` [85] to perform the hadronisation, showering and the subsequent analyses. All analyses except the search for soft leptons have been validated using the cutflows provided by the experimental collaborations, see appendix B. For the soft lepton CMS search, we use the validated `Rivet` [86] analysis `CMS_2018_I1646260` from within `PYTHIA`. For the CMS searches, we determine the limits on the cross sections by means of a $\mathrm{CL_s}$ method while for the ATLAS search we use the model independent limits provided for each bin.

Finally, regarding the muon anomalous magnetic moment a_μ we consider the two scenarios where it either exhibits an anomaly or is SM-like. For the first scenario we use the central value and uncertainty of $\Delta a_\mu^{\mathrm{exp,dat}}$ as given in equation (3.3), while we use the value for $\Delta a_\mu^{\mathrm{exp,lat}}$ given in equation (3.4) in the latter.

Results. The results of our global analysis are gathered in figure 5, figure 6 and figure 7. In figure 5(a) we show the allowed region in the η–λ_H plane at $95\,\%$ CL. The difference between the theory prediction of a_μ and its measurement is assumed to be given by equation (3.3), i.e. we consider a_μ^{exp} to exhibit an anomaly. The blue contour shows the case $\lambda_H < 0$ while the orange contour shows $\lambda_H > 0$. We find that NP effects in a_μ large enough to be compatible with $\Delta a_\mu^{\mathrm{exp,dat}}$ at $95\,\%$ CL can only be generated for positive lepton portal mass corrections. As discussed in section 2.2 and given in equation (2.6), these corrections are parameterised by η, which is found positive in figure 5(a). We also find that in our case the Higgs portal coupling is restricted to $-0.1 \lesssim \lambda_H \lesssim 0.01$. For negative λ_H the contributions to DM-nucleon scattering from the lepton and Higgs portal can interfere destructively, opening more parameter space and allowing for larger absolute values of λ_H than for the case of pure Higgs portal DM [29, 30]. If on the other hand λ_H is positive, we re-encounter

| (a) η–λ_H plane | (b) m_ψ–m_{ϕ_3} plane |
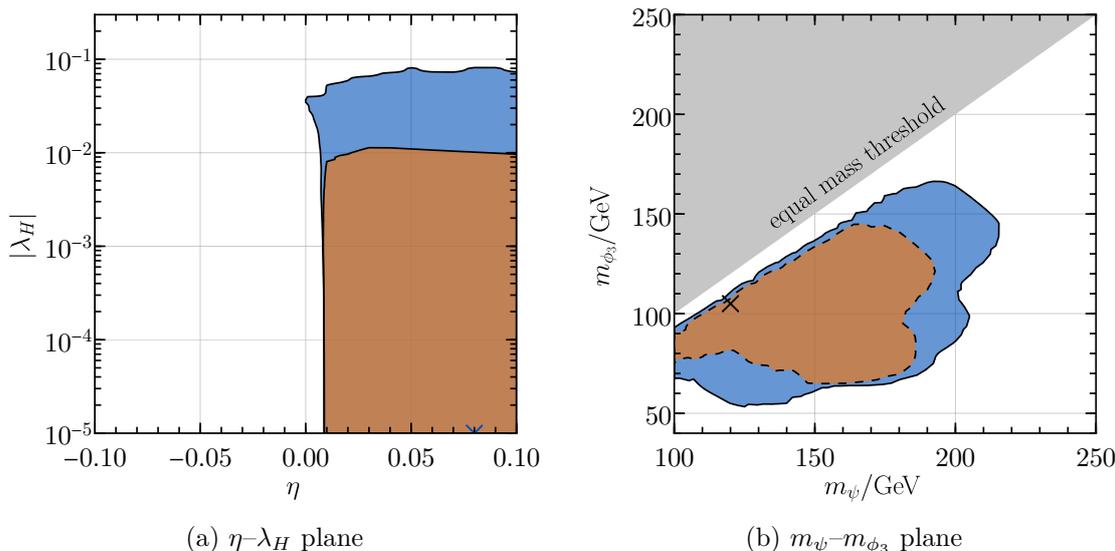
Figure 5. Correlation between fundamental model parameters when satisfying all constraints at given statistical significance considering an anomaly in $\Delta a_\mu^{\mathrm{exp}}$. The left panel shows the allowed regions at $95\,\%$ CL in the η–λ_H plane. The blue contour corresponds to the case $\lambda_H < 0$ and the orange contour shows $\lambda_H > 0$. In the right panel we show the allowed regions at $68\,\%$ CL (orange) and $95\,\%$ CL (blue) in the m_ψ–m_{ϕ_3} plane. In both panels the cross indicates the best-fit point.

the upper bound of $\lambda_H < 0.01$ known from the phenomenology of singlet scalar Higgs portal DM [29, 30]. This in turn means that the hierarchy between the different dark states is mainly driven by the lepton portal mass corrections, i.e. we obtain

$$m_{\phi_i}^2 \approx m_\phi{}^2 \left(1 + \eta\, D_j^2\right) , \qquad (3.8)$$

where the correspondence between the indices i and j is determined by the hierarchy of the couplings D_i and our convention $m_{\phi_1} > m_{\phi_2} > m_{\phi_3}$. Hence, for a positive parameter η the lightest and therefore stable state ϕ_3 couples with the smallest D_i. In addition, this coupling can become very small such that stringent constraints from direct and indirect detection can always be satisfied. The correct relic density can then be obtained through annihilations of the heavier states ϕ_1 and ϕ_2 alone. For negative λ_H, the afore-mentioned destructive interference allows for comparably strong Higgs portal interactions, such that annihilations of the fields ϕ_i into gauge bosons can also contribute to the freeze-out. In these parts of the parameter space, even the smallest of the couplings D_i can be of order $\mathcal{O}(1)$. We conclude that in spite of extending the parameter space to include NP scales of order $\mathcal{O}(100\,\mathrm{GeV})$, allowing non-vanishing Higgs portal interactions in the model studied in ref. [23] alone is not sufficient in order to explain the $(g-2)_\mu$ anomaly. It is rather necessary to consider the case $\eta > 0$, such that the hierarchy between the DM masses and couplings is inverted. This can also be inferred from the best-fit point,[7] which is obtained for $(\eta, \lambda_H) = (0.08, -10^{-5})$, i.e. the Higgs portal interactions alone do not resolve the anomaly in $\Delta a_\mu^{\mathrm{exp,dat}}$.

---

[7]Note that here we specifically refer to the best-fit point within the plotted plane. While the best-fit point is the same for all other planes where λ_H is free to float, here the value for λ_H can always fall on the lower limit of the logarithmic range as the true best fit is realised for $\lambda_H \to 0$ or very close to zero.

In figure 5(b) we show the allowed regions in the plane formed by the NP masses m_ψ and m_{ϕ_3} at 68 % CL (orange) and 95 % CL (blue), respectively, again considering an anomaly in a_μ. The lower right edge of both contours is due to exclusions coming from the collider search of ref. [76]. For the 2σ contour for instance, this edge would consist of a roughly straight line from $120\,\text{GeV} < m_\psi < 220\,\text{GeV}$, if only positive couplings λ_H were allowed. Above this line the allowed points typically exhibit a hierarchy where the DM-muon and DM-electron couplings[8] are close to maximal, while the DM-tau coupling is close to zero. Hence, the constraints from the observed relic density are satisfied by annihilations of ϕ_1 and ϕ_2 while direct detection limits are evaded due to the arbitrarily small DM-tau coupling. For smaller DM masses, i.e. allowed points below this line, the two contributions to the spin-independent DM-nucleon scattering cross section from lepton and Higgs portal processes interfere destructively. This opens up additional parameter space, in which the Higgs portal and DM-tau coupling can be comparatively large. Also, the DM-electron coupling does not necessarily need to be large and can even become smaller than the DM-tau coupling, since the annihilation rate is enhanced by Higgs portal interactions. Hence, one is always left with a non-negligible branching ratio of the mediator into τ-flavoured final states, which relaxes the collider constraints in this regime. The upper left edge close to the equal mass threshold $m_\psi = m_{\phi_3}$ is due to constraints from the observed DM relic density and $(g-2)_\mu$. In this regime the number density of the mediator ψ receives a weaker Boltzmann suppression, such that the freeze-out is dominated by $\psi\bar\psi$ s-wave annihilations. Above this upper edge however, the Boltzmann suppression of n_ψ becomes even weaker, such that the $\psi\bar\psi$ annihilations are so enhanced that one needs small DM-muon couplings in order to satisfy the relic density constraint. Such small couplings on the other hand are not compatible with the $(g-2)_\mu$ bound. The upper right edge of the contours on the other hand is due to the bound from $\Delta a_\mu^{\text{exp}}$ and the fact that we have limited the couplings D_i to $D_i \in [0,3]$. At 95 % CL, mediator masses $m_\psi \gtrsim 215\,\text{GeV}$ require couplings $D_i > 3$ in order to not obtain a too small NP contribution Δa_μ and be compatible with $\Delta a_\mu^{\text{exp,dat}}$ as given in equation (3.3). Finally, the lower left edge of the contours is due to constraints on the Z–ℓ vertex corrections. At 68 % CL for instance, NP contributions to the Z–μ vertex grow too large for mediator masses $m_\psi \lesssim 140\,\text{GeV}$, since the relevant coupling[9] $|\lambda_{\mu i}|$ cannot become arbitrarily small due to constraints from the observed relic density and in order to not generate too small NP effects Δa_μ. Hence, within the region $120\,\text{GeV} \lesssim m_\psi \lesssim 140\,\text{GeV}$ the constraints can only be satisfied for an increasing DM mass m_{ϕ_3}, since the relevant loop function for the corrections to the Z–ℓ vertices becomes suppressed in the limit $m_{\phi_3} \to m_\psi$. For even smaller masses $m_\psi \lesssim 120\,\text{GeV}$ we find that the interplay between the Z–ℓ vertex corrections and the collider search in the soft mass region from ref. [74] only allows for a tiny band close to the upper edge which extends down to $m_\psi = 100\,\text{GeV}$. As indicated by the black cross in figure 5(b), the best-fit point is obtained for $(m_\psi, m_{\phi_3}) = (120, 105)\,\text{GeV}$ and yields $\chi^2/\text{ndf} = 6.09/7$. Thus, in summary we find that in our model the $(g-2)_\mu$ anomaly can be explained within the mass range $100\,\text{GeV} \lesssim m_\psi \lesssim 190\,\text{GeV}$ at 68 % CL and within the range $100\,\text{GeV} \lesssim m_\psi \lesssim 215\,\text{GeV}$ at 95 % CL.

---

[8]Here and in what follows, the term "DM-lepton coupling" collectively refers to the coupling of any of the three dark flavours ϕ_i to the lepton, rather than that of the stable DM candidate ϕ_3 alone.

[9]Remember that we work with the convention $m_{\phi_1} > m_{\phi_2} > m_{\phi_3}$.
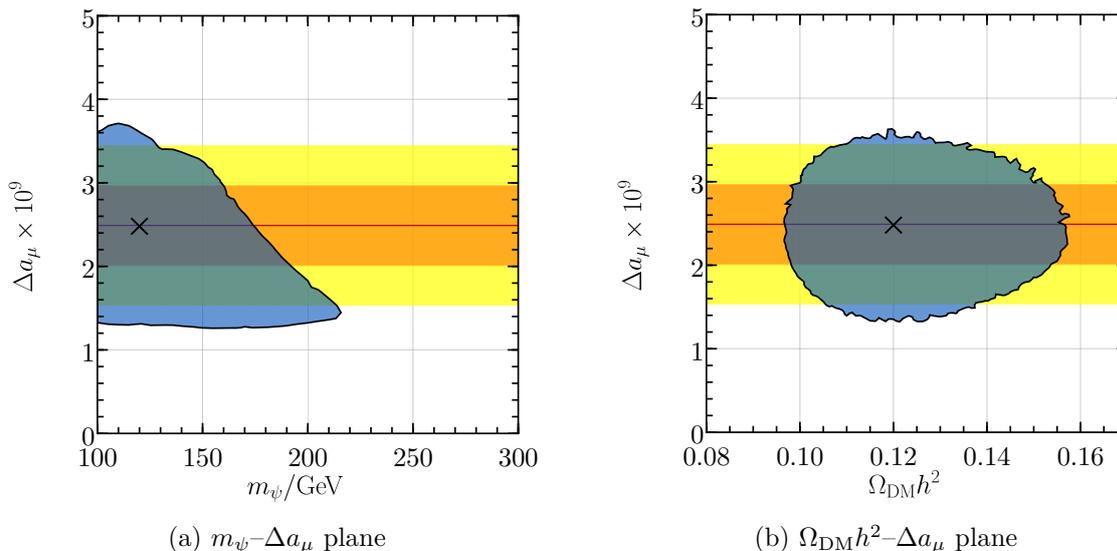
Figure 6. Correlation between NP effects in a_μ and model parameters or other observables when satisfying all constraints at 95 % CL considering an anomaly in $\Delta a_\mu^{\mathrm{exp}}$. In the left panel we show the allowed regions in the m_ψ–Δa_μ plane while the right panel shows the allowed regions in the $\Omega_{\mathrm{DM}}h^2$–Δa_μ plane. In both panels the black cross indicates the best-fit point, while the red, orange and yellow bands correspond to the central value and the 1σ and 2σ band of $\Delta a_\mu^{\mathrm{exp,dat}}$.

The correlation between NP effects in a_μ and the NP scale m_ψ when satisfying all constraints at 95 % CL is illustrated in figure 6(a). The lower edge of the allowed region here is directly related to $\Delta a_\mu^{\mathrm{exp,dat}}$ itself, while the steeply decreasing upper edge is due to the suppression of Δa_μ by the mediator mass m_ψ. Given that we have restricted the couplings D_i to $D_i \in [0,3]$, increasing mediator masses hence lead to smaller values of Δa_μ, as the DM-muon coupling cannot grow larger than $|\lambda_{\mu i}| = 3$. The decrease of the upper edge of the allowed values for Δa_μ for mediator masses $m_\psi \lesssim 120$ GeV is due to constraints on NP contributions to the Z–μ coupling, since in this regime the latter force the DM-muon coupling to satisfy $|\lambda_{\mu i}| < 3$. We find that the best fit is obtained for $\Delta a_\mu = 2.48 \times 10^{-9}$, i.e. the central value of $\Delta a_\mu^{\mathrm{exp,dat}}$ is precisely reproduced.

In figure 6(b) we show the correlation between the relic density of DM and NP effects in a_μ when satisfying all constraints at 95 % CL. The resulting region consists of an ellipse, which is stretched towards larger values of $\Omega_{\mathrm{DM}}h^2$. This indicates that there is no correlation between these two observables. The ellipse is stretched towards larger relic densities, since we assume an uncertainty of 10 % on the theory value of $\Omega_{\mathrm{DM}}h^2$, i.e. the uncertainty, and therefore the allowed region, grows with increasing central values. We find that the best fit also exactly reproduces the experimental central value of the DM relic density, i.e. $\Omega_{\mathrm{DM}}h^2 = 0.12$.

Finally, we also show the allowed regions in the NP mass plane, when the muon anomalous magnetic moment a_μ is considered to be SM-like in figure 7, using $\Delta a_\mu^{\mathrm{exp,lat}}$ from equation (3.4) in the fit. The orange region here shows the allowed parameter space at 95 % CL, while the blue region shows the corresponding region in the scenario in which a_μ is
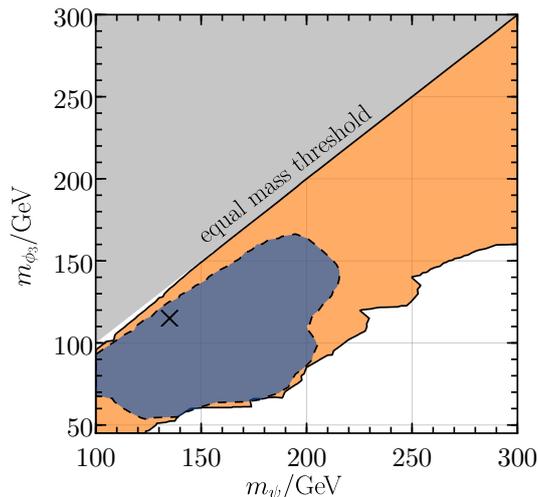
Figure 7. Correlation between m_ψ and m_{ϕ_3} when satisfying all constraints at $95\,\%$ CL. The orange region shows the allowed parameter space when considering a_μ to not exhibit an anomaly, i.e. we assume $\Delta a_\mu^{\mathrm{exp,lat}}$. The cross indicates the corresponding best-fit point. For comparison, the blue region shows the allowed masses when a_μ exhibits an anomaly.

considered to exhibit an anomaly. We find that the complete range of NP scales considered in our analysis is allowed. The viable parameter space is mainly determined by the relic density and collider constraints. Close to the near-degenerate region $m_\psi \approx m_{\phi_3}$ we find that the interplay between the soft searches from ref. [74] and relic density constraints excludes a tiny band for $m_\psi \lesssim 150\,\mathrm{GeV}$. Here, the restrictions from the mentioned search are so strong that they require couplings too small to comply with the relic density constraint. The lower edge of the orange region in figure 7, on the other hand, is due to similar reasons as the lower right edge of the contours in figure 5(a). Again, the allowed points close to this edge yield a destructive interference between Higgs and lepton portal contributions to the DM-nucleon scattering rate. Below this edge however, the collider constraints become so strong that in spite of this interference it is not possible to satisfy the relic density and collider constraints simultaneously. We further find that while it allows for a larger range of NP scales, this scenario does not yield a significantly better global description of experimental data. The best fit is obtained for $(m_\psi, m_{\phi_3}) = (135, 115)\,\mathrm{GeV}$ and yields a chi-squared of $\chi^2/\mathrm{ndf} = 5.93/7$, while the above-mentioned best fit of the anomaly-scenario yields $\chi^2/\mathrm{ndf} = 6.09/7$.

4   Summary

In this analysis we have studied a simplified model of flavoured complex scalar dark matter coupling to the SM through both the Higgs and lepton portals. To this end we have revisited the model presented in ref. [23], which extends the SM model by a complex scalar flavour triplet ϕ that couples to right-handed leptons ℓ_R through an electrically-charged vector-like Dirac fermion. The Higgs portal interactions, generally present in the model, were neglected in the analysis of ref. [23], and the hierarchy between the DM masses and couplings was

fixed in such a way that the lightest generation always has the largest coupling to the SM leptons. In this analysis we instead consider the most general case, by not only allowing for Higgs portal interactions but also by not constraining the hierarchy of DM couplings in any way aside from the chosen parameter ranges.

After presenting the model details and discussing its mass spectrum in section 2, we have outlined the fundamental phenomenological features of the Higgs portal interactions in section 3.1. Here we found that the main alterations of the phenomenology when comparing our results to the ones of ref. [23] are related to the production of DM in the early Universe and the phenomenology of DM detection experiments. The Higgs portal interactions give rise to several additional DM annihilation channels. Depending on the final state, this process can be resonantly enhanced at several mass thresholds, ultimately allowing for a much more dynamic production of DM than in the pure lepton portal scenario studied in ref. [23]. Similar findings also hold true for the model's direct detection phenomenology. A new contribution to spin-independent DM-nucleon scattering through the tree-level exchange of a Higgs boson in the t-channel turned out to destructively interfere with the lepton portal contribution in parts of the parameter space. Further, the new annihilation channels of DM into pairs of W or Z bosons or top quarks also renders indirect detection constraints from measurements of the anti-proton flux relevant. In spite of these new constraints, we found the parameter space of our model to be extended to include NP masses around the electroweak scale, which were originally excluded in ref. [23]. These small NP scales can either become viable through Higgs portal interactions only, while maintaining the hierarchy in the DM couplings from ref. [23], or by simply allowing for generic hierarchies.

Since, in contrast to the analysis of ref. [23], small enough NP scales to generate sizeable NP effects in the anomalous magnetic moment of the muon are allowed in our model, we have then discussed this observable in section 3.2. After outlining how different approaches to predict a_μ in the SM lead to significantly different results either exhibiting an anomaly or being compatible with the experimental measurement, we have concluded that the current situation requires further clarification and we thus consider both scenarios in our analysis. This section was then concluded by discussing the NP contributions Δa_μ generated within our model.

In section 3.3 we have then presented a combined analysis in which we determined our model's allowed parameter space by considering constraints from collider searches, the observed DM relic density, direct and indirect detection experiments, the electron anomalous magnetic moment, Z–ℓ vertex corrections and invisible Higgs decays. Regarding the anomalous magnetic moment of the muon a_μ we consider the two cases where it either exhibits an anomaly or is SM-like. In the former scenario we find that at the best-fit point both the central value of $\Delta a_\mu^{\text{exp}}$ and the correct DM relic density are precisely reproduced. The allowed NP scales are found to range from $m_\psi = 100\,\text{GeV}$ to $m_\psi = 215\,\text{GeV}$ at $95\,\%$ CL. For the scenario in which a_μ is SM-like we in contrast find the allowed NP scales to span over the complete range considered in our analysis. However, in spite of this larger allowed parameter space, within the EW scale the obtained best fit is not significantly better in this scenario and prefers similar masses.

In summary our results show that lepton-flavoured scalar DM can be realised at the EW scale and therefore in the reach of direct LHC searches. While such a low NP scale

also allows for a solution of the $(g-2)_\mu$ puzzle, we found the model to provide an equally viable DM candidate in case the latter observable eventually turns out to be SM-like.

Acknowledgments

A   Muon anomalous magnetic moment

The world-average of the experimental measurement of the anomalous magnetic moment of the muon reads [25–27]

$$a_\mu^{\mathrm{exp}} = (116592059 \pm 22) \times 10^{-11}\,. \tag{A.1}$$

Using dispersive techniques to extract the HVP contribution from $\sigma(\bar{e}e \to \mathrm{hadrons})$ data, the Muon $(g-2)_\mu$ Theory Initiative, based on [42–61], determined the SM prediction to be [28]

$$a_\mu^{\mathrm{SM,dat}} = (116591810 \pm 43) \times 10^{-11}\,. \tag{A.2}$$

Subtracting the leading-order HVP contribution from this prediction and replacing it by the BMW collaboration's lattice QCD prediction [62] yields a SM prediction which reads

$$a_\mu^{\mathrm{SM,lat}} = (116591954 \pm 58) \times 10^{-11}\,. \tag{A.3}$$

Other lattice calculations of the HVP contribution are consistent with the BMW result [63–66].

One last approach is to only use the lattice results for the so-called window observable a_μ^{win} [63], which is least prone to systematic uncertainties. The result for a_μ^{win} when again using data-driven techniques reads [68]

$$a_\mu^{\mathrm{win,dat}} = (2294 \pm 14) \times 10^{-11}\,, \tag{A.4}$$

whereas the lattice QCD world-average reads [67]

$$a_\mu^{\mathrm{win,lat}} = (2362 \pm 11) \times 10^{-11}\,. \tag{A.5}$$

Replacing only this window observable by its lattice QCD result in the leading-order HVP contribution as found by the Muon $(g-2)_\mu$ Theory Initiative [28] yields a total HVP contribution of

$$a_\mu^{\mathrm{HVP,dat+lat}} = (6999 \pm 38) \times 10^{-11}\,, \tag{A.6}$$

which when used to replace a_μ^{HVP} from the overall SM prediction presented in ref. [28] yields

$$a_\mu^{\mathrm{SM,dat+lat}} = (116591878 \pm 42) \times 10^{-11}\,. \tag{A.7}$$

The corresponding discrepancies between each theory prediction and the experimental measurement read

$$\Delta a_\mu^{\mathrm{exp,dat}} \quad = (2.49 \pm 0.48) \times 10^{-9}\,, \tag{A.8}$$

$$\Delta a_\mu^{\mathrm{exp,lat}} \quad = (1.05 \pm 0.62) \times 10^{-9}\,, \tag{A.9}$$

$$\Delta a_\mu^{\mathrm{exp,dat+lat}} = (1.81 \pm 0.47) \times 10^{-9}\,. \tag{A.10}$$

A brief summary of the current status of the $(g-2)_\mu$ SM prediction has recently been provided in refs. [87, 88].

B   Collider analysis

Here we present the implementation and validation of the recasts performed for the CMS and ATLAS searches presented in ref. [76] and ref. [75], respectively.

B.1   Validation of `PYTHIA` code for recasting arXiv:2012.08600 (CMS)

The CMS collaboration performed a search for supersymmetry in final states with two oppositely charged same-flavour (OCSF) leptons and missing transverse momentum at $\sqrt{s} = 13\,\mathrm{TeV}$ corresponding to an integrated luminosity of $137\,\mathrm{fb}^{-1}$ [76]. Note that we focus on the implementation of the slepton signal region since this is the topology corresponding to our model signal.

In order to define the signal regions, only same flavour leptons are used. Events are required to have two oppositely charged leptons within $|\eta| < 2.4$ (excluding the transition region between the barrel and endcap of the electromagnetic calorimeter $1.4 < |\eta| < 1.6$) and $p_{\mathrm{T}} > 50\,(20)\,\mathrm{GeV}$ for the highest (next-to-highest) p_{T} lepton. Selected leptons must be separated by a distance $\Delta R = \sqrt{(\Delta\eta)^2 + (\Delta\phi)^2} > 0.1$, with the azimuthal angle ϕ and pseudorapidity η. Further, in order to isolate the leptons from other particles in the event, the p_{T} sum of particle flow candidates in a cone ΔR around the lepton is required to be $< 10\,(20)\,\%$ of the electron (muon) p_{T}. The separation ΔR depends on the momentum of the lepton and is $\Delta R = 0.2$ for $p_{\mathrm{T}} < 50\,\mathrm{GeV}$, $\Delta R = 10\,\mathrm{GeV}/p_{\mathrm{T}}$ if $50\,\mathrm{GeV} < p_{\mathrm{T}} < 200\,\mathrm{GeV}$, and $\Delta R = 0.05$ otherwise. The invariant mass, $m_{\ell\ell}$, of the dilepton system, is required to be $< 65\,\mathrm{GeV}$ or $> 120\,\mathrm{GeV}$, its transverse momentum $p_T^{\ell\ell}$, and $p_{\mathrm{T}}^{\mathrm{miss}}$ are required to be greater than 50 and $100\,\mathrm{GeV}$, respectively. The variable $M_{\mathrm{T2}}(\ell\ell)$ is further required to be $M_{\mathrm{T2}}(\ell\ell) > 100\,\mathrm{GeV}$. It is defined as [89, 90]

$$M_{\mathrm{T2}} = \min_{\vec{p}_{\mathrm{T}}^{\mathrm{miss}(1)} + \vec{p}_{\mathrm{T}}^{\mathrm{miss}(2)} = \vec{p}_{\mathrm{T}}^{\mathrm{miss}}} \left[\max\left(M_{\mathrm{T}}^{(1)}, M_{\mathrm{T}}^{(2)} \right) \right]\,, \tag{B.1}$$

with the vector $\vec{p}_{\mathrm{T}}^{\mathrm{miss}(i)}, i = 1, 2$, in the transverse plane and the corresponding transverse mass $M_{\mathrm{T}}^{(i)}$ resulting from pairing the $\vec{p}_{\mathrm{T}}^{\mathrm{miss}(i)}$ with one of the two visible objects. Jets are clustered using the anti-k_T algorithm from `FastJet` [91] with a distance parameter of $R = 0.4$. Jets must lie within $|\eta| < 2.4$, have transverse momentum of $p_{\mathrm{T}} > 25\,\mathrm{GeV}$, and are removed if they lie within $\Delta R = 0.4$ of any selected lepton.

	(600, 0) GeV		(600, 400) GeV	
	Ref. [76]	this work	Ref. [76]	this work
Two OCSF leptons with $p_T > 25$ and $10\,\text{GeV}$	—	—	—	—
$p_T^{\ell\ell} > 50\,\text{GeV}$	98.4 %	98.2 %	95.1 %	95.0 %
$\Delta R(\ell\ell) > 0.1$	100 %	100 %	99.8 %	100 %
$m_{\ell\ell} < 65$ or $m_{\ell\ell} > 120\,\text{GeV}$	98.2 %	98.3 %	93.7 %	94.0 %
Leading lepton $p_T > 50\,\text{GeV}$	100 %	100 %	100 %	99.9 %
Third lepton veto	97.2 %	99.9 %	97.3 %	100 %
$M_{T2}(\ell\ell) > 100\,\text{GeV}$	83.0 %	83.5 %	69.4 %	69.6 %
$p_T^{\text{miss}} > 100\,\text{GeV}$	99.8 %	99.5 %	98.8 %	99.0 %
$n_j > 0$, $\Delta\phi(\vec{p}_T^{j_1}, \vec{p}_T^{\text{miss}}) > 0.4$ and $p_T^{\ell_2}/p_T^{j_1} > 1.2$	39.5 %	36.3 %	32.7 %	29.3 %
$n_j = 0$	43.7 %	46.2 %	44.6 %	47.2 %

Table 1. Cutflow for the slepton signal sample with the slepton-neutralino mass pair $(m_{\tilde{l}}, m_{\tilde{\chi}_1^0}) = (600, 0)\,\text{GeV}$ and $(600, 400)\,\text{GeV}$, respectively. The numbers correspond to the relative amount of events passing the respective cut.

The selected events are further split into two signal regions corresponding to zero and one additional jet, $n_j = 0, 1$. For the latter signal region the jet is required to have an angular separation $\Delta\phi$ from $\vec{p}_T^{\text{miss}}$ of $\Delta\phi(\vec{p}_T^{j_1}, \vec{p}_T^{\text{miss}}) > 0.4$ and transverse momentum of $p_T^{j_1} < p_T^{\ell_2}/1.2$. Finally, each signal region is further split into p_T^{miss} bins according to table 9 of ref. [76].

The analysis as just described has been implemented in `PYTHIA`. In order to calculate the variable $M_{T2}(\ell\ell)$, we use the implementation from ref. [92]. To verify our analysis, we generate a slepton signal sample with slepton-neutralino mass pairs $(m_{\tilde{l}}, m_{\tilde{\chi}_1^0})$ of $(600, 0)\,\text{GeV}$ and $(600, 400)\,\text{GeV}$ in `MadGraph5_aMC@NLO` at leading order. In table 1, we show the cutflow resulting from applying our analysis to the slepton signal sample and compare it to the cutflows taken from the auxiliary materials of the CMS analysis [76]. We show the number of events passing each cut relative to the number of events before applying it. The cuts are applied in the listed order. Note that we do not show the relative number of events passing the first cut as it depends on the event generation. We find excellent agreement with the CMS analysis [76].

B.2 Validation of `PYTHIA` code for recasting arXiv:2209.13935 (ATLAS)

ATLAS presented in ref. [75] a search for direct pair production of sleptons and charginos decaying to two leptons and neutralinos with mass splittings near the W-boson mass in $\sqrt{s} = 13\,\text{TeV}$ using $139\,\text{fb}^{-1}$ of collected data. Again, we only focus on the slepton search as this one corresponds to the topology of the model signal. Selected events have been divided into two signal regions (SR) corresponding to zero (SR-0J) and one (SR-1J) additional jets. Each signal region has further been divided into exclusive (binned) and inclusive signal regions in the stransverse mass M_{T2} as defined in appendix B.1. Note that we only use the inclusive signal regions to recast the search since for those ATLAS provides

Signal region (SR)	SR-0J	SR-1J
$n_{b\text{-tagged jets}}$	0	0
$E_{\mathrm{T}}^{\mathrm{miss}}$ significance	> 7	> 7
$n_{\text{non-}b\text{-tagged jets}}$	0	1
$p_{\mathrm{T}}^{\ell_1}$ in GeV	> 140	> 100
$p_{\mathrm{T}}^{\ell_2}$ in GeV	> 20	> 50
$m_{\ell\ell}$ in GeV	> 11	> 60
$p_{\mathrm{T,boost}}^{\ell\ell}$	< 5	—
$|\cos\theta_{\ell\ell}^*|$	< 0.2	< 0.1
$\Delta\phi_{\ell,\ell}$	> 2.2	> 2.8
$\Delta\phi_{p_{\mathrm{T}}^{\mathrm{miss}},\ell_1}$	> 2.2	—

Table 2. Selection criteria for the slepton search region of ref. [75]. See text for the definition of the variables.

the model-independent upper limits at 95 % CL on the observed number of beyond the SM events. The selection criteria are listed in table 2. In contrast to the CMS search in appendix B.1, jet candidates in the ATLAS search are removed if they lie within $\Delta R = 0.2$ of an electron candidate, or if they contain fewer than three tracks that lie within $\Delta R = 0.4$ of a muon candidate. Electrons and muons that lie within $\Delta R' = \min(0.4, 0.04 + 10/p_{\mathrm{T}})$ of the remaining jets are discarded. Note that also the lepton isolation criteria differ from the ones of the CMS search, cf. ref. [75]. In order to increase the sensitivity for the supersymmetric models, this search makes use of the variable $\cos\theta_{\ell\ell}^* = \tanh(\Delta\eta_{\ell\ell}/2)$ with the pseudorapidity difference between the two leptons $\Delta\eta_{\ell\ell}$. Additionally, the variable $E_{\mathrm{T}}^{\mathrm{miss}}$ significance is used to discriminate between undetected particles and poorly measured ones. The variable $E_{\mathrm{T}}^{\mathrm{miss}}$ significance is defined as [93]

$$E_{\mathrm{T}}^{\mathrm{miss}} \text{ significance} = \frac{|\vec{p}_{\mathrm{T}}^{\mathrm{miss}}|}{\sqrt{\sigma_{\mathrm{L}}^2(1 - \rho_{\mathrm{LT}}^2)}}\,, \tag{B.2}$$

with the negative vector sum of all identified particles $\vec{p}_{\mathrm{T}}^{\mathrm{miss}}$, the variable σ_{L} denoting the longitudinal component of the total transverse momentum resolution, and the correlation factor ρ_{LT} between the parallel and perpendicular components of the transverse momentum resolution for each object.

All selection criteria have been implemented in PYTHIA. To model the variable $E_{\mathrm{T}}^{\mathrm{miss}}$ significance, we use and digitise the information in ref. [93]. To calculate the stransverse mass M_{T2}, we use the implementation from ref. [92].

In order to validate the analysis, we generate a slepton signal sample in MadGraph5_aMC@NLO at leading order. The sample is generated for slepton masses of $m_{\tilde{l}} = 100\,\mathrm{GeV}$ and a neutralino mass of $m_{\tilde{\chi}_1^0} = 70\,\mathrm{GeV}$. The comparison of the resulting cutflows from our analysis with the ones provided by ATLAS, taken from the auxiliary materials of ref. [75], are shown in table 3. There, we show the number of events passing each cut relative to the number of events before applying the cut. Note that we do

	SR-0J		SR-1J	
	Ref. [75]	this work	Ref. [75]	this work
Events with only 2 leptons, with $p_\mathrm{T} > 9\,\mathrm{GeV}$	—	—	—	—
Trigger & $p_\mathrm{T}^{\ell_1} > 27\,\mathrm{GeV}$	82.1 %	86.3 %	82.1 %	86.3 %
$n_\mathrm{jet} < 2$	78.8 %	87.1 %	78.8 %	87.1 %
$p_\mathrm{T}^{\ell_2} > 20\,\mathrm{GeV}$	74.6 %	70.7 %	74.6 %	70.7 %
Events with same flavour leptons	100 %	100 %	100 %	100 %
Events with opposite sign leptons	99.5 %	100 %	99.5 %	100 %
$m_{\ell\ell} > 11\,\mathrm{GeV}$	100 %	100 %	100 %	100 %
$m_{\ell\ell} < 76\,\mathrm{GeV}$ or $m_{\ell\ell} > 106\,\mathrm{GeV}$	70.7 %	70.2 %	70.7 %	70.2 %
$E_\mathrm{T}^\mathrm{miss}$ significance > 7	9.36 %	8.96 %	9.36 %	8.96 %
$n_\mathrm{jet} = 0$	45.8 %	40.9 %	—	—
$p_{\mathrm{T,boost}}^{\ell\ell} < 5$	24.2 %	19.4 %	—	—
$\cos\theta_{\ell\ell}^* < 0.2$	38.7 %	38.1 %	—	—
$\Delta\phi_{p_\mathrm{T}^\mathrm{miss},\ell_1} > 2.2$	95.2 %	100 %	—	—
$\Delta\phi_{\ell\ell} > 2.2$	100 %	100 %	—	—
$p_T^{\ell_1} > 140\,\mathrm{GeV}$	49.7 %	55.4 %	—	—
$n_\mathrm{jet} = 1$	—	—	54.1 %	60.3 %
$n_\text{b-tagged jets} = 0$	—	—	95.5 %	98.4 %
$m_{\ell\ell} > 60$	—	—	86.0 %	84.9 %
$\cos\theta_{\ell\ell}^* < 0.1$	—	—	18.8 %	17.4 %
$\Delta\phi_{\ell\ell} > 2.2$	—	—	47.3 %	37.8 %
$p_T^{\ell_2} > 50\,\mathrm{GeV}$	—	—	61.6 %	55.0 %
$p_T^{\ell_1} > 100\,\mathrm{GeV}$	—	—	82.5 %	68.3 %

Table 3. Cutflow for the mass pair $(m_{\tilde{\ell}}, m_{\tilde{\chi}_1^0}) = (100, 70)\,\mathrm{GeV}$ for the signal regions SR-0J and SR-1J. The numbers correspond to the relative amount of events passing each cut.

not show the relative number of events passing the first cut as it depends on the event generation. In conclusion, we find good agreement with the analysis performed by the ATLAS collaboration.

References

[1] S. Profumo, L. Giani and O.F. Piattella, *An Introduction to Particle Dark Matter*, *Universe* **5** (2019) 213 [arXiv:1910.05610] [INSPIRE].

[2] A. Arbey and F. Mahmoudi, *Dark matter and the early Universe: a review*, *Prog. Part. Nucl. Phys.* **119** (2021) 103865 [arXiv:2104.11488] [INSPIRE].

[3] J. Kile and A. Soni, *Flavored Dark Matter in Direct Detection Experiments and at LHC*, *Phys. Rev. D* **84** (2011) 035016 [arXiv:1104.5239] [INSPIRE].

[4] J.F. Kamenik and J. Zupan, *Discovering Dark Matter Through Flavor Violation at the LHC*, *Phys. Rev. D* **84** (2011) 111502 [arXiv:1107.0623] [INSPIRE].

[5] B. Batell, J. Pradler and M. Spannowsky, *Dark Matter from Minimal Flavor Violation*, *JHEP* **08** (2011) 038 [arXiv:1105.1781] [INSPIRE].

[6] P. Agrawal, S. Blanchet, Z. Chacko and C. Kilic, *Flavored Dark Matter, and Its Implications for Direct Detection and Colliders*, *Phys. Rev. D* **86** (2012) 055002 [arXiv:1109.3516] [INSPIRE].

[7] B. Batell, T. Lin and L.-T. Wang, *Flavored Dark Matter and R-Parity Violation*, *JHEP* **01** (2014) 075 [arXiv:1309.4462] [INSPIRE].

[8] J. Kile, *Flavored Dark Matter: A Review*, *Mod. Phys. Lett. A* **28** (2013) 1330031 [arXiv:1308.0584] [INSPIRE].

[9] J. Kile, A. Kobach and A. Soni, *Lepton-Flavored Dark Matter*, *Phys. Lett. B* **744** (2015) 330 [arXiv:1411.1407] [INSPIRE].

[10] L. Lopez-Honorez and L. Merlo, *Dark matter within the minimal flavour violation ansatz*, *Phys. Lett. B* **722** (2013) 135 [arXiv:1303.1087] [INSPIRE].

[11] A.J. Buras et al., *Universal unitarity triangle and physics beyond the standard model*, *Phys. Lett. B* **500** (2001) 161 [hep-ph/0007085] [INSPIRE].

[12] G. D'Ambrosio, G.F. Giudice, G. Isidori and A. Strumia, *Minimal flavor violation: An effective field theory approach*, *Nucl. Phys. B* **645** (2002) 155 [hep-ph/0207036] [INSPIRE].

[13] A.J. Buras, *Minimal flavor violation*, *Acta Phys. Polon. B* **34** (2003) 5615 [hep-ph/0310208] [INSPIRE].

[14] R.S. Chivukula and H. Georgi, *Composite Technicolor Standard Model*, *Phys. Lett. B* **188** (1987) 99 [INSPIRE].

[15] L.J. Hall and L. Randall, *Weak scale effective supersymmetry*, *Phys. Rev. Lett.* **65** (1990) 2939 [INSPIRE].

[16] V. Cirigliano, B. Grinstein, G. Isidori and M.B. Wise, *Minimal flavor violation in the lepton sector*, *Nucl. Phys. B* **728** (2005) 121 [hep-ph/0507001] [INSPIRE].

[17] P. Agrawal, M. Blanke and K. Gemmler, *Flavored dark matter beyond Minimal Flavor Violation*, *JHEP* **10** (2014) 072 [arXiv:1405.6709] [INSPIRE].

[18] M. Blanke and S. Kast, *Top-Flavoured Dark Matter in Dark Minimal Flavour Violation*, *JHEP* **05** (2017) 162 [arXiv:1702.08457] [INSPIRE].

[19] M. Blanke, S. Das and S. Kast, *Flavoured Dark Matter Moving Left*, *JHEP* **02** (2018) 105 [arXiv:1711.10493] [INSPIRE].

[20] T. Jubb, M. Kirk and A. Lenz, *Charming Dark Matter*, *JHEP* **12** (2017) 010 [arXiv:1709.01930] [INSPIRE].

[21] H. Acaroğlu and M. Blanke, *Tasting flavoured Majorana dark matter*, *JHEP* **05** (2022) 086 [arXiv:2109.10357] [INSPIRE].

[22] M.-C. Chen, J. Huang and V. Takhistov, *Beyond Minimal Lepton Flavored Dark Matter*, *JHEP* **02** (2016) 060 [arXiv:1510.04694] [INSPIRE].

[23] H. Acaroğlu, P. Agrawal and M. Blanke, *Lepton-flavoured scalar dark matter in Dark Minimal Flavour Violation*, *JHEP* **05** (2023) 106 [arXiv:2211.03809] [INSPIRE].

[24] H. Acaroğlu, P. Agrawal and M. Blanke, *Flavoured $(g-2)_\mu$ with Dark Lepton Seasoning*, *SciPost Phys.* **15** (2023) 176 [arXiv:2212.08142] [INSPIRE].

[25] MUON G-2 collaboration, *Final Report of the Muon E821 Anomalous Magnetic Moment Measurement at BNL*, *Phys. Rev. D* **73** (2006) 072003 [hep-ex/0602035] [INSPIRE].

[26] MUON G-2 collaboration, *Measurement of the Positive Muon Anomalous Magnetic Moment to 0.46 ppm*, *Phys. Rev. Lett.* **126** (2021) 141801 [arXiv:2104.03281] [INSPIRE].

[27] MUON G-2 collaboration, *Measurement of the Positive Muon Anomalous Magnetic Moment to 0.20 ppm*, *Phys. Rev. Lett.* **131** (2023) 161802 [arXiv:2308.06230] [INSPIRE].

[28] T. Aoyama et al., *The anomalous magnetic moment of the muon in the Standard Model*, *Phys. Rept.* **887** (2020) 1 [arXiv:2006.04822] [INSPIRE].

[29] J.M. Cline, K. Kainulainen, P. Scott and C. Weniger, *Update on scalar singlet dark matter*, *Phys. Rev. D* **88** (2013) 055025 [*Erratum ibid.* **92** (2015) 039906] [arXiv:1306.4710] [INSPIRE].

[30] GAMBIT collaboration, *Status of the scalar singlet dark matter model*, *Eur. Phys. J. C* **77** (2017) 568 [arXiv:1705.07931] [INSPIRE].

[31] M. Blanke et al., *Another look at the flavour structure of the littlest Higgs model with T-parity*, *Phys. Lett. B* **646** (2007) 253 [hep-ph/0609284] [INSPIRE].

[32] A. Cuoco, J. Heisig, M. Korsmeier and M. Krämer, *Constraining heavy dark matter with cosmic-ray antiprotons*, *JCAP* **04** (2018) 004 [arXiv:1711.05274] [INSPIRE].

[33] A. Cuoco, M. Krämer and M. Korsmeier, *Novel Dark Matter Constraints from Antiprotons in Light of AMS-02*, *Phys. Rev. Lett.* **118** (2017) 191102 [arXiv:1610.03071] [INSPIRE].

[34] M. Tavakoli, I. Cholis, C. Evoli and P. Ullio, *Constraints on Dark Matter Annihilations from Diffuse Gamma-Ray Emission in the Galaxy*, *JCAP* **01** (2014) 017 [arXiv:1308.4135] [INSPIRE].

[35] MEG collaboration, *Search for the lepton flavour violating decay $\mu^+ \to e^+\gamma$ with the full dataset of the MEG experiment*, *Eur. Phys. J. C* **76** (2016) 434 [arXiv:1605.05081] [INSPIRE].

[36] BABAR collaboration, *Searches for Lepton Flavor Violation in the Decays $\tau^\pm \to e^\pm\gamma$ and $\tau^\pm \to \mu^\pm\gamma$*, *Phys. Rev. Lett.* **104** (2010) 021802 [arXiv:0908.2381] [INSPIRE].

[37] BELLE collaboration, *Search for lepton-flavor-violating tau-lepton decays to $\ell\gamma$ at Belle*, *JHEP* **10** (2021) 019 [arXiv:2103.12994] [INSPIRE].

[38] PLANCK collaboration, *Planck 2018 results. VI. Cosmological parameters*, *Astron. Astrophys.* **641** (2020) A6 [*Erratum ibid.* **652** (2021) C4] [arXiv:1807.06209] [INSPIRE].

[39] LZ collaboration, *First Dark Matter Search Results from the LUX-ZEPLIN (LZ) Experiment*, *Phys. Rev. Lett.* **131** (2023) 041002 [arXiv:2207.03764] [INSPIRE].

[40] A. Ibarra, A.S. Lamperstorfer and J. Silk, *Dark matter annihilations and decays after the AMS-02 positron measurements*, *Phys. Rev. D* **89** (2014) 063539 [arXiv:1309.2570] [INSPIRE].

[41] M. Garny, A. Ibarra, M. Pato and S. Vogl, *Internal bremsstrahlung signatures in light of direct dark matter searches*, *JCAP* **12** (2013) 046 [arXiv:1306.6342] [INSPIRE].

[42] T. Aoyama, M. Hayakawa, T. Kinoshita and M. Nio, *Complete Tenth-Order QED Contribution to the Muon g-2*, *Phys. Rev. Lett.* **109** (2012) 111808 [arXiv:1205.5370] [INSPIRE].

[43] T. Aoyama, T. Kinoshita and M. Nio, *Theory of the Anomalous Magnetic Moment of the Electron*, *Atoms* **7** (2019) 28 [INSPIRE].

[44] A. Czarnecki, W.J. Marciano and A. Vainshtein, *Refinements in electroweak contributions to the muon anomalous magnetic moment*, *Phys. Rev. D* **67** (2003) 073006 [*Erratum ibid.* **73** (2006) 119901] [hep-ph/0212229] [INSPIRE].

[45] C. Gnendiger, D. Stöckinger and H. Stöckinger-Kim, *The electroweak contributions to $(g-2)_\mu$ after the Higgs boson mass measurement*, *Phys. Rev. D* **88** (2013) 053005 [arXiv:1306.5546] [INSPIRE].

[46] M. Davier, A. Hoecker, B. Malaescu and Z. Zhang, *Reevaluation of the hadronic vacuum polarisation contributions to the Standard Model predictions of the muon $g-2$ and $\alpha(m_Z^2)$ using newest hadronic cross-section data*, *Eur. Phys. J. C* **77** (2017) 827 [arXiv:1706.09436] [INSPIRE].

[47] A. Keshavarzi, D. Nomura and T. Teubner, *Muon $g-2$ and $\alpha(M_Z^2)$: a new data-based analysis*, *Phys. Rev. D* **97** (2018) 114025 [arXiv:1802.02995] [INSPIRE].

[48] G. Colangelo, M. Hoferichter and P. Stoffer, *Two-pion contribution to hadronic vacuum polarization*, *JHEP* **02** (2019) 006 [arXiv:1810.00007] [INSPIRE].

[49] M. Hoferichter, B.-L. Hoid and B. Kubis, *Three-pion contribution to hadronic vacuum polarization*, *JHEP* **08** (2019) 137 [arXiv:1907.01556] [INSPIRE].

[50] M. Davier, A. Hoecker, B. Malaescu and Z. Zhang, *A new evaluation of the hadronic vacuum polarisation contributions to the muon anomalous magnetic moment and to $\alpha(m_Z^2)$*, *Eur. Phys. J. C* **80** (2020) 241 [*Erratum ibid.* **80** (2020) 410] [arXiv:1908.00921] [INSPIRE].

[51] A. Keshavarzi, D. Nomura and T. Teubner, *$g-2$ of charged leptons, $\alpha(M_Z^2)$, and the hyperfine splitting of muonium*, *Phys. Rev. D* **101** (2020) 014029 [arXiv:1911.00367] [INSPIRE].

[52] A. Kurz, T. Liu, P. Marquard and M. Steinhauser, *Hadronic contribution to the muon anomalous magnetic moment to next-to-next-to-leading order*, *Phys. Lett. B* **734** (2014) 144 [arXiv:1403.6400] [INSPIRE].

[53] K. Melnikov and A. Vainshtein, *Hadronic light-by-light scattering contribution to the muon anomalous magnetic moment revisited*, *Phys. Rev. D* **70** (2004) 113006 [hep-ph/0312226] [INSPIRE].

[54] P. Masjuan and P. Sanchez-Puertas, *Pseudoscalar-pole contribution to the $(g_\mu - 2)$: a rational approach*, *Phys. Rev. D* **95** (2017) 054026 [arXiv:1701.05829] [INSPIRE].

[55] G. Colangelo, M. Hoferichter, M. Procura and P. Stoffer, *Dispersion relation for hadronic light-by-light scattering: two-pion contributions*, *JHEP* **04** (2017) 161 [arXiv:1702.07347] [INSPIRE].

[56] M. Hoferichter et al., *Dispersion relation for hadronic light-by-light scattering: pion pole*, *JHEP* **10** (2018) 141 [arXiv:1808.04823] [INSPIRE].

[57] A. Gérardin, H.B. Meyer and A. Nyffeler, *Lattice calculation of the pion transition form factor with $N_f = 2+1$ Wilson quarks*, *Phys. Rev. D* **100** (2019) 034520 [arXiv:1903.09471] [INSPIRE].

[58] J. Bijnens, N. Hermansson-Truedsson and A. Rodríguez-Sánchez, *Short-distance constraints for the HLbL contribution to the muon anomalous magnetic moment*, *Phys. Lett. B* **798** (2019) 134994 [arXiv:1908.03331] [INSPIRE].

[59] G. Colangelo et al., *Longitudinal short-distance constraints for the hadronic light-by-light contribution to* $(g-2)_\mu$ *with large-N_c Regge models*, *JHEP* **03** (2020) 101 [arXiv:1910.13432] [INSPIRE].

[60] T. Blum et al., *Hadronic Light-by-Light Scattering Contribution to the Muon Anomalous Magnetic Moment from Lattice QCD*, *Phys. Rev. Lett.* **124** (2020) 132002 [arXiv:1911.08123] [INSPIRE].

[61] G. Colangelo et al., *Remarks on higher-order hadronic corrections to the muon g-2*, *Phys. Lett. B* **735** (2014) 90 [arXiv:1403.7512] [INSPIRE].

[62] S. Borsanyi et al., *Leading hadronic contribution to the muon magnetic moment from lattice QCD*, *Nature* **593** (2021) 51 [arXiv:2002.12347] [INSPIRE].

[63] M. Cè et al., *Window observable for the hadronic vacuum polarization contribution to the muon g-2 from lattice QCD*, *Phys. Rev. D* **106** (2022) 114502 [arXiv:2206.06582] [INSPIRE].

[64] EXTENDED TWISTED MASS collaboration, *Lattice calculation of the short and intermediate time-distance hadronic vacuum polarization contributions to the muon magnetic moment using twisted-mass fermions*, *Phys. Rev. D* **107** (2023) 074506 [arXiv:2206.15084] [INSPIRE].

[65] FERMILAB LATTICE et al. collaborations, *Light-quark connected intermediate-window contributions to the muon g-2 hadronic vacuum polarization from lattice QCD*, *Phys. Rev. D* **107** (2023) 114514 [arXiv:2301.08274] [INSPIRE].

[66] RBC and UKQCD collaborations, *An update of Euclidean windows of the hadronic vacuum polarization*, *Phys. Rev. D* **108** (2023) 054507 [arXiv:2301.08696] [INSPIRE].

[67] H. Wittig, *Progress on* $(g-2)_\mu$ *from Lattice QCD*, in the proceedings of the *57th Rencontres de Moriond on Electroweak Interactions and Unified Theories*, La Thuile, Italy, 18–25 March 2023 [arXiv:2306.04165] [INSPIRE].

[68] G. Colangelo et al., *Data-driven evaluations of Euclidean windows to scrutinize hadronic vacuum polarization*, *Phys. Lett. B* **833** (2022) 137313 [arXiv:2205.12963] [INSPIRE].

[69] CMD-3 collaboration, *Measurement of the* $e^+e^- \to \pi^+\pi^-$ *cross section from threshold to 1.2 GeV with the CMD-3 detector*, arXiv:2302.08834 [INSPIRE].

[70] CMD-2 collaboration, *Reanalysis of hadronic cross-section measurements at CMD-2*, *Phys. Lett. B* **578** (2004) 285 [hep-ex/0308008] [INSPIRE].

[71] KLOE-2 collaboration, *Combination of KLOE* $\sigma\left(e^+e^- \to \pi^+\pi^-\gamma(\gamma)\right)$ *measurements and determination of* $a_\mu^{\pi^+\pi^-}$ *in the energy range* $0.10 < s < 0.95\,GeV^2$, *JHEP* **03** (2018) 173 [arXiv:1711.03085] [INSPIRE].

[72] BESIII collaboration, *Measurement of the* $e^+e^- \to \pi^+\pi^-$ *cross section between 600 and 900 MeV using initial state radiation*, *Phys. Lett. B* **753** (2016) 629 [*Erratum ibid.* **812** (2021) 135982] [arXiv:1507.08188] [INSPIRE].

[73] BABAR collaboration, *Precise Measurement of the* $e^+e^- \to \pi^+\pi^-(\gamma)$ *Cross Section with the Initial-State Radiation Method at BABAR*, *Phys. Rev. D* **86** (2012) 032013 [arXiv:1205.2228] [INSPIRE].

[74] CMS collaboration, *Search for new physics in events with two soft oppositely charged leptons and missing transverse momentum in proton-proton collisions at $\sqrt{s} = 13$ TeV*, *Phys. Lett. B* **782** (2018) 440 [arXiv:1801.01846] [INSPIRE].

[75] ATLAS collaboration, *Search for direct pair production of sleptons and charginos decaying to two leptons and neutralinos with mass splittings near the W-boson mass in $\sqrt{s} = 13$ TeV pp collisions with the ATLAS detector*, *JHEP* **06** (2023) 031 [arXiv:2209.13935] [INSPIRE].

[76] CMS collaboration, *Search for supersymmetry in final states with two oppositely charged same-flavor leptons and missing transverse momentum in proton-proton collisions at $\sqrt{s} = 13$ TeV*, *JHEP* **04** (2021) 123 [arXiv:2012.08600] [INSPIRE].

[77] D. Hanneke, S. Fogwell and G. Gabrielse, *New Measurement of the Electron Magnetic Moment and the Fine Structure Constant*, *Phys. Rev. Lett.* **100** (2008) 120801 [arXiv:0801.1134] [INSPIRE].

[78] L. Morel, Z. Yao, P. Cladé and S. Guellati-Khélifa, *Determination of the fine-structure constant with an accuracy of 81 parts per trillion*, *Nature* **588** (2020) 61 [INSPIRE].

[79] T. Aoyama, M. Hayakawa, T. Kinoshita and M. Nio, *Tenth-Order QED Contribution to the Electron g-2 and an Improved Value of the Fine Structure Constant*, *Phys. Rev. Lett.* **109** (2012) 111807 [arXiv:1205.5368] [INSPIRE].

[80] ALEPH et al. collaborations, *Precision electroweak measurements on the Z resonance*, *Phys. Rept.* **427** (2006) 257 [hep-ex/0509008] [INSPIRE].

[81] ATLAS collaboration, *A detailed map of Higgs boson interactions by the ATLAS experiment ten years after the discovery*, *Nature* **607** (2022) 52 [*Erratum ibid.* **612** (2022) E24] [arXiv:2207.00092] [INSPIRE].

[82] G. Bélanger et al., *microMEGAs5.0: Freeze-in*, *Comput. Phys. Commun.* **231** (2018) 173 [arXiv:1801.03509] [INSPIRE].

[83] J. Alwall et al., *The automated computation of tree-level and next-to-leading order differential cross sections, and their matching to parton shower simulations*, *JHEP* **07** (2014) 079 [arXiv:1405.0301] [INSPIRE].

[84] A. Alloul et al., *FeynRules 2.0 — A complete toolbox for tree-level phenomenology*, *Comput. Phys. Commun.* **185** (2014) 2250 [arXiv:1310.1921] [INSPIRE].

[85] C. Bierlich et al., *A comprehensive guide to the physics and usage of PYTHIA 8.3*, arXiv:2203.11601 [DOI:10.21468/SciPostPhysCodeb.8] [INSPIRE].

[86] C. Bierlich et al., *Robust Independent Validation of Experiment and Theory: Rivet version 3*, *SciPost Phys.* **8** (2020) 026 [arXiv:1912.05451] [INSPIRE].

[87] G. Colangelo, M. Hoferichter and P. Stoffer, *Puzzles in the hadronic contributions to the muon anomalous magnetic moment*, in the proceedings of the *21st Conference on Flavor Physics and CP Violation*, Lyon, France, 29 May – 02 June 2023 [arXiv:2308.04217] [INSPIRE].

[88] MUON G-2 THEORY INITIATIVE collaboration, *The Status of Muon $g-2$ Theory in the Standard Model*, https://muon-gm2-theory.illinois.edu/.

[89] C.G. Lester and D.J. Summers, *Measuring masses of semiinvisibly decaying particles pair produced at hadron colliders*, *Phys. Lett. B* **463** (1999) 99 [hep-ph/9906349] [INSPIRE].

[90] A. Barr, C. Lester and P. Stephens, *m(T2): The truth behind the glamour*, *J. Phys. G* **29** (2003) 2343 [hep-ph/0304226] [INSPIRE].

[91] M. Cacciari, G.P. Salam and G. Soyez, *FastJet User Manual*, *Eur. Phys. J. C* **72** (2012) 1896 [arXiv:1111.6097] [ɪɴSPIRE].

[92] C.G. Lester and B. Nachman, *Bisection-based asymmetric M_{T2} computation: a higher precision calculator than existing symmetric methods*, *JHEP* **03** (2015) 100 [arXiv:1411.4312] [ɪɴSPIRE].

[93] ATLAS collaboration, *Object-based missing transverse momentum significance in the ATLAS detector*, ATLAS-CONF-2018-038, CERN, Geneva (2018).